arXiv:1701.03567v1 [cond-mat.supr-con] 13 Jan 2017

Dynamics of quenched topological edge modes

P. D. Sacramento*

Departamento de Física and CeFEMA,
Instituto Superior Técnico, Universidade de Lisboa,
Av. Rovisco Pais, 1049-001 Lisboa, Portugal
**E-mail: pdss@cefema-gt.tecnico.ulisboa.pt*

A characteristic feature of topological systems is the presence of robust gapless edge states. In this work the effect of time-dependent perturbations on the edge states is considered. Specifically we consider perturbations that can be understood as changes of the parameters of the Hamiltonian. These changes may be sudden or carried out at a fixed rate. In general, the edge modes decay in the thermodynamic limit, but for finite systems a revival time is found that scales with the system size. The dynamics of fermionic edge modes and Majorana modes are compared. The effect of periodic perturbations is also referred allowing the appearance of edge modes out of a topologically trivial phase.

Keywords: Topology; time-dependent perturbations.

1. Sudden quantum quenches

An example of a time-dependent transformation of the Hamiltonian is a sudden change of its parameters. Let us consider an Hamiltonian defined by an initial set of parameters ξ_0 for times $t < t_0$. The single-particle eigenstates of the Hamiltonian are given by

$$H(\xi_0)|\psi_{m_0}(\xi_0)\rangle = E_{m_0}(\xi_0)|\psi_{m_0}(\xi_0)\rangle, \tag{1}$$

where m_0 are the quantum numbers. At time $t = t_0$ a sudden transformation of the parameters is performed, $\xi_0 \to \xi_1$. The Hamiltonian eigenstates transform to

$$H(\xi_1)|\psi_{m_1}(\xi_1)\rangle = E_{m_1}(\xi_1)|\psi_{m_1}(\xi_1)\rangle. \tag{2}$$

After this sudden quench the system will evolve in time under the influence of a different Hamiltonian. The time evolution of a single-particle state,

with quantum number m_0, is given by

$$|\psi^I_{m_0}(t)\rangle = \sum_{m_1} e^{-iE_{m_1}(\xi_1)(t-t_0)} |\psi_{m_1}(\xi_1)\rangle\langle\psi_{m_1}(\xi_1)|\psi_{m_0}(\xi_0)\rangle \tag{3}$$

for times $t \geq t_0$. The survival probability of some initial state $|\psi_{m_0}(\xi_0)\rangle$ is defined by

$$P_{m_0}(t) = |\langle\psi_{m_0}(\xi_0)|\psi^I_{m_0}(t)\rangle|^2. \tag{4}$$

We will be interested in the fate of single particle states after a quantum quench across the phase diagram. We consider a subspace of one excitation such that the total Hamiltonian is given by the ground state energy plus one excited state and assume we remain in the one excitation subspace after the quench. In this work only unitary evolution of single-particle states is considered and effects of dissipation are neglected.

We may as well consider further quenches defined in a sequence of times and sets of parameters as $t_0 < t_1 < t_2 < t_3 < \cdots$ and $\xi_0, \xi_1, \xi_2, \xi_3, \cdots$, respectively. These intervals define regions as $I(t_0 \leq t < t_1), II(t_1 \leq t < t_2), III(t_2 \leq t < t_3), \cdots$. The case of a single quench is clearly obtained taking $t_1 \to \infty$, and so on for further quenches ($t_0 = 0$ is chosen hereafter).

Consider now a case for which we have two quenches in succession. In this case we have that the evolution of the initial state with quantum number m_0 is

$$\begin{aligned}
|\psi^{II}_{m_0}(t)\rangle &= e^{-iH(\xi_2)(t-t_1)}|\psi^I_{m_0}(t_1)\rangle \\
&= \sum_{m_2} e^{-iE_{m_2}(\xi_2)(t-t_1)} |\psi_{m_2}(\xi_2)\rangle\langle\psi_{m_2}(\xi_2)|\psi^I_{m_0}(t_1)\rangle \\
&= \sum_{m_2}\sum_{m_1} e^{-iE_{m_2}(\xi_2)(t-t_1)} e^{-iE_{m_1}(\xi_1)t_1} \\
&\quad |\psi_{m_2}(\xi_2)\rangle\langle\psi_{m_2}(\xi_2)|\psi_{m_1}(\xi_1)\rangle\langle\psi_{m_1}(\xi_1)|\psi_{m_0}(\xi_0)\rangle
\end{aligned} \tag{5}$$

Choosing $\xi_2 = \xi_0$ we get that for $t_1 \leq t < \infty$ ($t_2 \to \infty$) the overlap with an initial state, n_0, is given by

$$\langle\psi_{n_0}(\xi_0)|\psi^{II}_{m_0}(t)\rangle = \sum_{m_1} e^{-iE_{n_0}(\xi_0)(t-t_1)} e^{-iE_{m_1}(\xi_1)t_1} \langle\psi_{n_0}(\xi_0)|\psi_{m_1}(\xi_1)\rangle\langle\psi_{m_1}(\xi_1)|\psi_{m_0}(\xi_0)\rangle \tag{6}$$

Therefore, the probability to find a projection to an initial state, n_0, given that the initial state is m_0 is given by

$$\begin{aligned} P_{n_0 m_0}(t) &= |\langle \psi_{n_0}(\xi_0)|\psi^{II}_{m_0}(t)\rangle|^2 \\ &= |\sum_{m_1} e^{-iE_{m_1}(\xi_1)t_1} \\ &\quad \langle \psi_{n_0}(\xi_0)|\psi_{m_1}(\xi_1)\rangle\langle\psi_{m_1}(\xi_1)|\psi_{m_0}(\xi_0)\rangle|^2, \end{aligned} \tag{7}$$

which is independent of time.

We may now at some given finite time, t_2, change the parameters from $\xi_2 \to \xi_3$. As before we find that for $t_2 \leq t < \infty$ the same probability as in eq. (7) is given by

$$P_{n_0 m_0}(t) = |\langle \psi_{n_0}(\xi_0)|\psi^{III}_{m_0}(t)\rangle|^2 \tag{8}$$

where

$$|\psi^{III}_{m_0}(t)\rangle = e^{-iH(\xi_3)(t-t_2)}|\psi^{II}_{m_0}(t_2)\rangle \tag{9}$$

The probability is now a function of time.

2. Models

In this chapter we consider systems that are topologically non-trivial, such as one or two-dimensional topological insulators or topological superconductors. The topological nature of these systems reveals itself both in the topological nature of the groundstate of the infinite system and in the appearance of edge states if the system is finite (bulk-edge correspondance). Different topological invariants may be defined such as winding numbers for the one-dimensional examples considered here and the Chern number for the two-dimensional superconductor considered later. Both the winding numbers and the Chern number may be understood in various ways [1–3] and typically they count the number of edge modes at the interface between the topological system and the vacuum.

Some examples are the models considered in this section which display both trivial and topological phases. The dynamics of the edge modes of the topological phases after a quantum quench is considered in sections 3-5.

2.1. *One-band spinless superconductor: the 1D Kitaev model*

The Kitaev one-dimensional superconductor with triplet p-wave pairing is described by the Hamiltonian[4]

$$H = \sum_{j=1}^{\bar{N}} \left[-\tilde{t} \left(c_j^\dagger c_{j+1} + c_{j+1}^\dagger c_j \right) + \Delta \left(c_j c_{j+1} + c_{j+1}^\dagger c_j^\dagger \right) \right] - \sum_{j=1}^{N} \mu \left(c_j^\dagger c_j - \frac{1}{2} \right) \tag{10}$$

where $\bar{N} = N$ if we use periodic boundary conditions (and $N + 1 = 1$) or $\bar{N} = N - 1$ if we use open boundary conditions. Here N is the number of sites. $\tilde{t}$ is the hopping amplitude taken as the unit of energy, Δ is the pairing amplitude and μ the chemical potential. The operator c_j destroys a spinless fermion at site j.

In momentum space the model is written as

$$\hat{H} = \frac{1}{2} \sum_k \left(c_k^\dagger, c_{-k} \right) H_k \begin{pmatrix} c_k \\ c_{-k}^\dagger \end{pmatrix} \tag{11}$$

where

$$H_k = \begin{pmatrix} \epsilon_k - \mu & i\Delta \sin k \\ -i\Delta \sin k & -\epsilon_k + \mu \end{pmatrix} \tag{12}$$

with $\epsilon_k = -2\tilde{t} \cos k$. Here c_k is the Fourier transform of c_j.

In general, a fermion operator may be writen in terms of two hermitian operators, γ_1, γ_2, in the following way

$$\begin{aligned} c_{j,\sigma} &= \frac{1}{2} \left(\gamma_{j,\sigma,1} + i\gamma_{j,\sigma,2} \right) \\ c_{j,\sigma}^\dagger &= \frac{1}{2} \left(\gamma_{j,\sigma,1} - i\gamma_{j,\sigma,2} \right) \end{aligned} \tag{13}$$

The index σ represents internal degrees of freedom of the fermionic operator, such as spin and/or sublattice index, the γ operators are hermitian and satisfy a Clifford algebra

$$\{\gamma_m, \gamma_n\} = 2\delta_{nm}. \tag{14}$$

In the case of the Kitaev model it is enough to consider $c_j = (\gamma_{j,1} + i\gamma_{j,2})/2$, since the fermions are spinless. In terms of these hermitian (Majorana) operators we may write that the Hamiltonian is given by, using open boundary

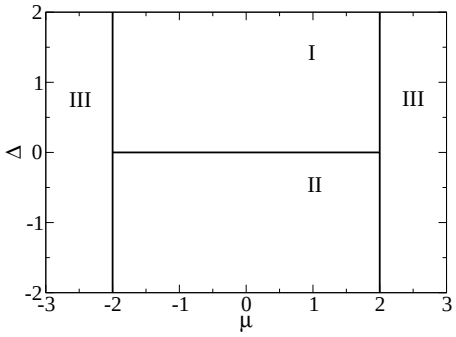

Fig. 1. Phase diagram of $1D$ Kitaev model. In phases I and II there are edge modes.

conditions,

$$H = \frac{i}{2}\sum_{j=1}^{N-1}\left[(-\tilde{t}+\Delta)\gamma_{j,1}\gamma_{j+1,2} + (\tilde{t}+\Delta)\gamma_{j,2}\gamma_{j+1,1}\right] - \frac{i}{2}\sum_{j=1}^{N}\mu\gamma_{j,1}\gamma_{j,2} \tag{15}$$

Taking $\mu = 0$ and selecting the special point $\tilde{t} = \Delta$ the Hamiltonian simplifies considerably to

$$H(\mu = 0, \tilde{t} = \Delta) = i\tilde{t}\sum_{j=1}^{N-1}\gamma_{j,2}\gamma_{j+1,1} = -i\tilde{t}\sum_{j=1}^{N-1}\gamma_{j+1,1}\gamma_{j,2} \tag{16}$$

Note that the operators $\gamma_{1,1}$ and $\gamma_{N,2}$ are missing from the Hamiltonian. Therefore there are two zero energy modes. Defining from these two Majorana fermions a single usual fermion operator (non-hermitian), taking one of the Majorana operators as the real part and the other as the imaginary part, its state may be either occupied or empty with no cost in energy. Defining $d_j = 1/2\,(\gamma_{j,2} + i\gamma_{j+1,1})$ and $d_N = 1/2\,(\gamma_{N,2} + i\gamma_{1,1})$ we can write the Hamiltonian as

$$H = \tilde{t}\sum_{j=1}^{N-1}\left(2d_j^\dagger d_j - 1\right) + \epsilon_N\left(2d_N^\dagger d_N - 1\right) \tag{17}$$

with $\epsilon_N = 0$. Therefore the fermionic mode d_N does not appear in the Hamiltonian and the state may be occuppied or empty ($d_N^\dagger d_N = 1, 0$, re-

spectively) with no energy cost. These two states are therefore degenerate in energy and are perfectly localized at the edges of the chain as δ-function peaks (with exponential accuracy as the system size grows).

The phase diagram of the Kitaev model shows three types of phases (see Fig. 1): two topological phases in which there are gapless edge modes, if the system is finite, and two trivial phases with no edge modes. In the various phases the bulk of the system is gapped and at the transition lines the gap closes, allowing the possibility of a change of topology. The transition lines are located at $\Delta = 0, |\mu| \leq 2\tilde{t}$ and at $|\mu| = 2\tilde{t}$ and any Δ.

2.2. *Multiband system: 1D Two-band Shockley model*

The Shockley model is a model of a dimerized system of spinless fermions with alternating nearest-neighbor hoppings, given by the Hamiltonian (see for instance[3])

$$H = \sum_{j=1}^{N} \psi^\dagger(j) \left[U\psi(j) + V\psi(j-1) + V^\dagger\psi(j+1) \right) \tag{18}$$

where the 2×2 matrices U and V and the spinor ψ representing two orbitals at site j that are hybridized by the matrices U and V are given by

$$U = \begin{pmatrix} 0 & t_1^* \\ t_1 & 0 \end{pmatrix}; V = \begin{pmatrix} 0 & t_2^* \\ 0 & 0 \end{pmatrix}; \psi(j) = \begin{pmatrix} c_{j,A} \\ c_{j,B} \end{pmatrix}. \tag{19}$$

t_1 and t_2 are hoppings and $c_{j,A}$ ($c_{j,B}$) destroy spinless fermions at site j belonging to sublattice A (B), respectively.

We may as well define Majorana operators as

$$\begin{aligned} c_{j,A} &= \frac{1}{2}\left(\gamma_{j,A,1} + i\gamma_{j,A,2}\right) \\ c_{j,B} &= \frac{1}{2}\left(\gamma_{j,B,1} + i\gamma_{j,B,2}\right) \end{aligned} \tag{20}$$

Here A and B take the role of pseudospins. Taking t_1 and t_2 real, the

Hamiltonian may be written as

$$\begin{aligned} H = & \frac{it_1}{2}\sum_{j=1}^{N}(\gamma_{j,A,1}\gamma_{j,B,2}+\gamma_{j,B,1}\gamma_{j,A,2}) \\ & + \frac{t_2}{4}\sum_{j=2}^{N}(\gamma_{j,A,1}\gamma_{j-1,B,1}+\gamma_{j,A,2}\gamma_{j-1,B,2}) \\ & + \frac{it_2}{4}\sum_{j=2}^{N}(\gamma_{j,A,1}\gamma_{j-1,B,2}-i\gamma_{j,A,2}\gamma_{j-1,B,1}) \\ & + \frac{t_2}{4}\sum_{j=1}^{N-1}(\gamma_{j,B,1}\gamma_{j+1,A,1}+\gamma_{j,B,2}\gamma_{j+1,A,2}) \\ & + \frac{it_2}{4}\sum_{j=1}^{N-1}(\gamma_{j,B,1}\gamma_{j+1,A,2}-i\gamma_{j,B,2}\gamma_{j+1,A,1}) \end{aligned} \tag{21}$$

Choosing $t_1 = 0$ we find that the Majorana fermions $\gamma_{1,A,1}$, $\gamma_{1,A,2}$, $\gamma_{N,B,1}$ and $\gamma_{N,B,2}$ do not contribute and are zero energy modes. These decoupled zero-energy modes are fermionic in nature, since the decoupled Majoranas are located at the two end sites, A and B, respectively. This point is characteristic of the topological phase as long as the bulk gap does not vanish. In the trivial phase there are no decoupled Majorana operators. As discussed for instance in Ref.[3] the two types of phases may also be distinguished by the winding number.

2.3. *Multiband system: 1D SSH model with triplet pairing*

This model may be viewed as a dimerized Kitaev superconductor[5]. The dimerization is parametrized by η and the superconductivity by Δ.

This model is given by the Hamiltonian

$$\begin{aligned} H = & -\mu\sum_j\left(c^\dagger_{j,A}c_{j,A}+c^\dagger_{j,B}c_{j,B}\right) \\ & -\tilde{t}\sum_j\Big[(1+\eta)c^\dagger_{j,B}c_{j,A}+(1+\eta)c^\dagger_{j,A}c_{j,B} \\ & \quad + \ (1-\eta)c^\dagger_{j+1,A}c_{j,B}+(1-\eta)c^\dagger_{j,B}c_{j+1,A}\Big] \\ & +\Delta\sum_j\Big[(1+\eta)c^\dagger_{j,B}c^\dagger_{j,A}+(1+\eta)c_{j,A}c_{j,B} \\ & \quad + \ (1-\eta)c^\dagger_{j+1,A}c^\dagger_{j,B}+(1-\eta)c_{j,B}c_{j+1,A}\Big] \end{aligned} \tag{22}$$

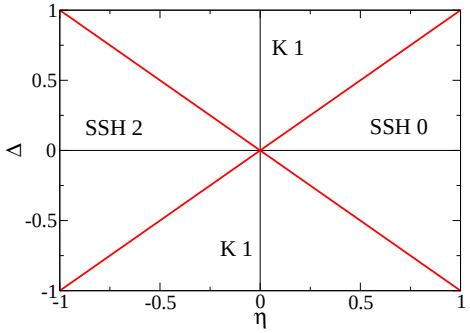

Fig. 2. (Color online) Phase diagram of $1D$ SSH-Kitaev model for $\mu = 0$. The phase SSH0 is trivial and has no edge modes. In the phases K1 there is one edge Majorana mode at each edge and in the phase SSH2 there are fermionic edge modes at each edge

($\tilde{t}$ is the hopping, Δ the pairing amplitude and μ the chemical potential). The model with no superconductivity ($\Delta = 0$) is related to the Shockley model taking $t_1 = \tilde{t}(1+\eta)$ and $t_2 = \tilde{t}(1-\eta)$. The region of $\eta > 0$ corresponds to $t_1 > t_2$ and vice-versa for $\eta < 0$. The Hamiltonian in real space mixes nearest-neighbor sites and also has local terms.

In terms of Majorana operators the Hamiltonian is written as

$$\begin{aligned} H = & -\frac{\mu}{2}\sum_{j=1}^{N}(2 + i\gamma_{j,A,1}\gamma_{j,A,2} + i\gamma_{j,B,1}\gamma_{j,B,2}) \\ & - \frac{i\tilde{t}}{2}(1+\eta)\sum_{j=1}^{N}(\gamma_{j,B,1}\gamma_{j,A,2} + \gamma_{j,A,1}\gamma_{j,B,2}) \\ & - \frac{i\tilde{t}}{2}(1-\eta)\sum_{j=1}^{N-1}(\gamma_{j+1,A,1}\gamma_{j,B,2} + \gamma_{j,B,1}\gamma_{j+1,A,2}) \\ & + \frac{i\Delta}{2}(1+\eta)\sum_{j=1}^{N}(\gamma_{j,A,1}\gamma_{j,B,2} + \gamma_{j,A,2}\gamma_{j,B,1}) \\ & + \frac{i\Delta}{2}(1-\eta)\sum_{j=1}^{N-1}(\gamma_{j,B,1}\gamma_{j+1,A,2} + \gamma_{j,B,2}\gamma_{j+1,A,1}) \end{aligned} \tag{23}$$

Consider once again a vanishing chemical potential. Taking $\eta = -1$

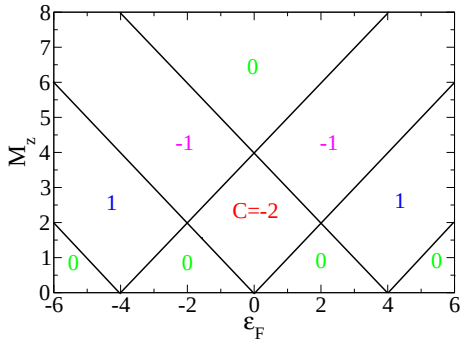

Fig. 3. (Color online) Phase diagram of $2D$ p-wave model as a function of the chemical potential and magnetization. C is the Chern number of each phase associated with the number of protected one-dimensional edge modes at finite magnetization.

and $\Delta = 0$ we have a state similar to the SSH or Shockley models with two fermionic-like zero energy edge states, since the four operators $\gamma_{1,A,1}, \gamma_{1,A,2}; \gamma_{N,B,1}, \gamma_{N,B,2}$ are missing from the Hamiltonian. If we select $\eta = 0$ and $t = \Delta$ is a Kitaev like state since there are two Majorana operators missing from the Hamiltonian, $\gamma_{1,A,1}$ and $\gamma_{N,B,2}$, one from each end. An example of a trivial phase is the point $\eta = 1$ and $\Delta = 0$ in which case there are no zero energy edge states. In Fig. 2 the phase diagram is shown. This model provides a testing ground for the comparison between fermionic and Majorana edge modes. In addition, in some regimes it displays finite energy modes that are localized at the edges of the chain, as obtained before in other multiband models[6].

2.4. *Two-dimensional spinfull triplet superconductor*

Another interesting case is that of a two-dimensional triplet superconductor with p-wave symmetry, spin-orbit coupling and a Zeeman term[7]. We write the Hamiltonian for the bulk system in momentum space as

$$\hat{H} = \frac{1}{2}\sum_{\boldsymbol{k}} \left(\boldsymbol{\psi}^{\dagger}_{\boldsymbol{k}}, \boldsymbol{\psi}_{-\boldsymbol{k}}\right) \begin{pmatrix} \hat{H}_0(\boldsymbol{k}) & \hat{\Delta}(\boldsymbol{k}) \\ \hat{\Delta}^{\dagger}(\boldsymbol{k}) & -\hat{H}_0^T(-\boldsymbol{k}) \end{pmatrix} \begin{pmatrix} \boldsymbol{\psi}_{\boldsymbol{k}} \\ \boldsymbol{\psi}^{\dagger}_{-\boldsymbol{k}} \end{pmatrix} \tag{24}$$

where $\left(\boldsymbol{\psi}^{\dagger}_{\boldsymbol{k}}, \boldsymbol{\psi}_{-\boldsymbol{k}}\right) = \left(\psi^{\dagger}_{\boldsymbol{k}\uparrow}, \psi^{\dagger}_{\boldsymbol{k}\downarrow}, \psi_{-\boldsymbol{k}\uparrow}, \psi_{-\boldsymbol{k}\downarrow}\right)$ and

$$\hat{H}_0 = \epsilon_{\boldsymbol{k}}\sigma_0 - M_z\sigma_z + \hat{H}_R\,. \tag{25}$$

Here, $\epsilon_{\boldsymbol{k}} = -2\tilde{t}(\cos k_x + \cos k_y) - \varepsilon_F$ is the kinetic part, $\tilde{t}$ denotes the hopping parameter set in the following as the energy scale ($\tilde{t} = 1$), $\boldsymbol{k}$ is a wave vector in the xy plane, and we have taken the lattice constant to be unity. Furthermore, M_z is the Zeeman splitting term responsible for the magnetization, in $\tilde{t}$ units. The Rashba spin-orbit term is written as

$$\hat{H}_R = \boldsymbol{s} \cdot \boldsymbol{\sigma} = \alpha \left(\sin k_y \sigma_x - \sin k_x \sigma_y \right) , \tag{26}$$

where α is measured in the same units and $\boldsymbol{s} = \alpha(\sin k_y, -\sin k_x, 0)$. The matrices $\sigma_x, \sigma_y, \sigma_z$ are the Pauli matrices acting on the spin sector, and σ_0 is the 2×2 identity. The pairing matrix reads

$$\hat{\Delta} = i \left(\boldsymbol{d} \cdot \boldsymbol{\sigma} \right) \sigma_y = \begin{pmatrix} -d_x + i d_y & d_z \\ d_z & d_x + i d_y \end{pmatrix} . \tag{27}$$

We consider here $d_z = 0$. If the spin-orbit coupling is strong it is energetically favorable that the pairing is of the form $\boldsymbol{d} = d\boldsymbol{s}$.

The energy eigenvalues and eigenfunction may be obtained solving the Bogoliubov-de Gennes equations

$$\begin{pmatrix} \hat{H}_0(\boldsymbol{k}) & \hat{\Delta}(\boldsymbol{k}) \\ \hat{\Delta}^\dagger(\boldsymbol{k}) & -\hat{H}_0^T(-\boldsymbol{k}) \end{pmatrix} \begin{pmatrix} u_n \\ v_n \end{pmatrix} = \epsilon_{\boldsymbol{k},n} \begin{pmatrix} u_n \\ v_n \end{pmatrix} . \tag{28}$$

The 4-component spinor can be written as

$$\begin{pmatrix} u_n \\ v_n \end{pmatrix} = \begin{pmatrix} u_n(\boldsymbol{k}, \uparrow) \\ u_n(\boldsymbol{k}, \downarrow) \\ v_n(-\boldsymbol{k}, \uparrow) \\ v_n(-\boldsymbol{k}, \downarrow) \end{pmatrix} . \tag{29}$$

The superconductor we consider here is time-reversal invariant if the Zeeman term is absent. The system then belongs to the symmetry class DIII where the topological invariant is a $\mathbb{Z}_2$ index[8]. If the Zeeman term is finite, time reversal symmetry (TRS) is broken and the system belongs to the symmetry class D. The topological invariant that characterizes this phase is the first Chern number C, and the system is said to be a $\mathbb{Z}$ topological superconductor. The phase diagram is shown in Fig. 3.

Due to the bulk-edge correspondence if the system is placed in a strip geometry and the system is in a topologically non-trivial phase, there are robust edge states, in a number of pairs given by the Chern number, if time reversal symmetry is broken. There are also counterpropagating edge states in the Z_2 phases even though the Chern number vanishes, as in the spin Hall effect. In these phases time reversal symmetry is preserved and

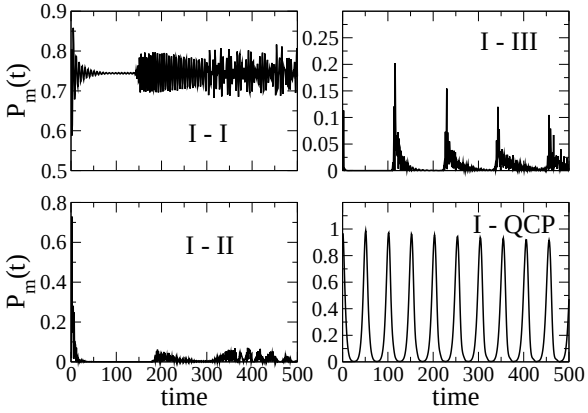

Fig. 4. Survival probability of the Majorana state of the one-dimensional Kitaev model for different transitions across the phase diagram: i) transition within the same topological phase, I, $(\mu = 0.5, \Delta = 0.6) \rightarrow (\mu = 1.0, \Delta = 0.6)$, ii) transition from the topological phase I to the trivial phase III $(\mu = 0.5, \Delta = 0.6) \rightarrow (\mu = 2.2, \Delta = 0.6)$, iii) transition from the topological phase I with positive Δ to the topological phase I with negative Δ $(\mu = 0.5, \Delta = 0.6) \rightarrow (\mu = 0.5, \Delta = -0.6)$, iv) transition within the same topological phase, I, to the quantum critical point $(\mu = 0, \Delta = 0.1) \rightarrow (\mu = 0, \Delta = 0)$ where the system is gapless. The system has 100 sites. Reproduced from Ref. [10].

the Kramers pairs of edge states give opposite contributions to the Chern number. Interestingly, turning on the magnetization (Zeeman field) time reversal symmetry is broken and the edge states are no longer topologically protected. However, it was found that, even in regimes where $C = 0$, there are edge states, reminiscent of the edge states of the Z_2 phases.

3. Dynamics of edge modes of 1D Kitaev model

3.1. *Single quench*

The stability of the Majorana fermions in this model has been considered recently [9]. In Fig. 4 we present results for the survival probability of the Majorana mode for different quenches [10]. In the first panel we consider the case of a quench within the same topological phase clearly showing that the survival probability is finite. Since the parameters change, there is a decrease of $P(t)$ as a function of time due to the overlap with *all* the eigenstates of the chain with the new set of parameters, but after some

oscillations the survival rate stabilizes at some finite value. As time grows, oscillations appear again centered around some finite value. Therefore the Majorana mode is robust to the quench. In the second panel we consider a quench from the topological phase I to the trivial, non-topological phase III. The behavior is quite different. After the quench the survival probability decays fast to nearly zero. After some time it increases sharply and repeats the decay and revival process. Similar results are found for a quench between the two topological phases I and II. As discussed in ref.[9] the revival time scales with the system size. At this instant the wave function is peaked around the center of the system and is the result of a propagating mode across the system with a given velocity and, therefore, scales with the system size. In the infinite system limit the revival time will diverge and the Majorana mode decays and is destroyed. A qualitatively different case is illustrated in the last panel of Fig. 2 where a quench from the topological phase I to the quantum critical point at the origin is considered.

Let us analyse these oscillations in greater detail. Consider first $\mu = 0$ and quenches where one varies Δ, or a fixed Δ and changing μ. In the case of $\mu = 0$ the critical point is located at $\mu = 0, \Delta = 0$ and in the second case there is a line of critical points at $\mu = 2\tilde{t}$. One finds that there is a point that separates the existence or not of oscillations. If the initial state is close enough to the critical point there are oscillations. Otherwise they are absent. For instance, in the quench from the topological phase I to the critical point at $\mu = 0, \Delta = 0$, the point is located as $N = 100, \Delta = 0.34$, $N = 200, \Delta = 0.18$, $N = 400, 0.05 < \Delta < 0.1$. In the vicinity of the two critical lines of points (around $\mu = 2\tilde{t}, \Delta = 0$), no matter how close the initial point is to the critical line, one does not find oscillations (for further details see ref.[11]).

In Fig. 5 the survival probability, $P(t)$, of a Majorana mode as a function of time, for various critical quenches is presented. In the first panel are shown the oscillations of $P(t)$ as one quenches from a given value of Δ to the critical point $\mu = 0, \Delta = 0$, maintaining $\mu = 0$. For small deviations of the initial value of Δ from the critical point, $P(t)$ is close to 1 and as one increases the distance from the critical point the amplitude decreases considerably. The oscillations are quite smooth and clear until the amplitude has decreased enough to reach zero. Beyond this point there is a periodicity but no longer oscillations since there are increasing regions where $P(t)$ basically vanishes. In this case it seems more like the revival times of non-critical quenches, even though the curves are still smooth. Beyond a given value of Δ_d there is a *period doubling*. Also, after this period

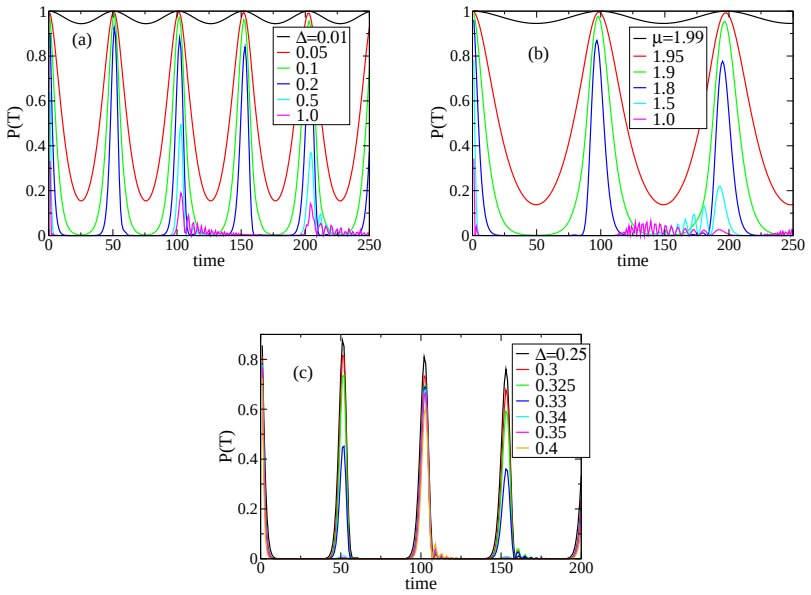

Fig. 5. (Color online) Survival probability, $P(t)$, of a Majorana mode in the $1D$ Kitaev model as one approaches critical points. In panel (c) the crossover to period doubling is shown as one approaches the critical region. The system size is $N = 100$. In (a) $\mu = 0$, in (b) $\Delta = 0.5$, and in (c) $\mu = 0$. Reproduced from Ref. [11].

doubling the survival probability looses its regular periodic behavior and shows more oscillations of smaller periods and amplitude decays that are similar to results previously found in quenches away from critical points [9,10]. In the second panel are shown quenches to the critical line $\mu = 2\tilde{t}$ keeping $\Delta = 0.5$ and decreasing the chemical potential. The behavior is similar to the first panel. In the third panel is shown in greater detail the *crossover* to period doubling for the transition to the critical point. The point of crossover, Δ_d, scales linearly with $1/N$.

The survival probability is determined by the various energies of the final Hamiltonian eigenstates and their overlaps to the initial single-particle state. In Fig. 6 the overlaps between the initial lowest energy state (Majorana mode) and all the final state eigenvectors are shown, as a function of their energies, for $N = 200$. In general, the overlaps are peaked at the lowest energies. There is a clear separation of regimes as one reaches the crossover region where the period doubling occurs. At small values of Δ

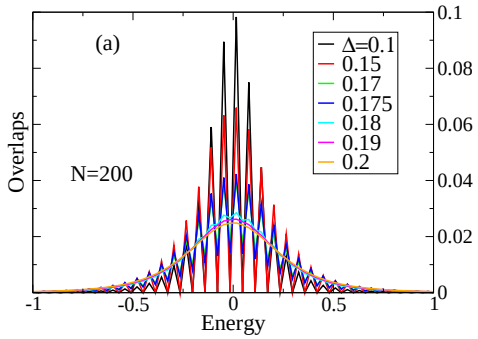

Fig. 6. (Color online) Overlaps for the $1D$ Kitaev model as a function of energy. The critical point is $\mu = 0, \Delta = 0$. Reproduced from Ref. [11].

the overlaps oscillate between finite and zero values. This is a parity effect distinguishing even and odd number of sites. It can be noted that the overlaps are very sharp around the lowest energy states. As the crossover occurs the overlaps are no longer zero at some energy eigenvalues and actually become very smooth. This means that the contributions from the various energy states changes, the time behavior is affected and the clean oscillations are no longer observed. In order to have clean oscillations one needs contributions from few energy levels. A perfect oscillation requires finite overlaps to two states and the frequency of the oscillations is the difference in their energy values. In general, the overlaps have very different magnitudes to the two states and the period of oscillations shown in $P(t)$ depends on their magnitudes. Adding significant contributions from other energy eigenstates leads first to modulated oscillations and then to a complicated time dependence.

The origin of the period doubling is understood in the following way. In Fig. 7 the time evolution of the Majorana state is shown, for a critical quench from a region far from the critical point where the period has doubled, and a quench from the region of oscillations, close to the critical point. In the first case the wave functions at each edge are separated in two energy modes while for the second they are mixed. This is due to the long range correlations close to the critical point that effectively decrease the system size and lead to the coupling of the two edge modes. In the first case the time evolved states from each edge cross each other in a solitonic

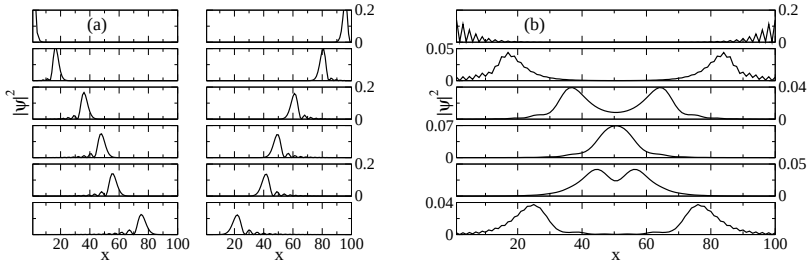

Fig. 7. Solitonic-like vs. constructive interference behavior of the wave functions in the $1D$ Kitaev model. In (a) the initial state is far from the critical point (CP) and in (b)one is close to the CP. In (a) the quench takes place from $\mu = 0, \Delta = 0.5$ to $\mu = 0, \Delta = 0$ and in (b) from $\mu = 0, \Delta = 0.1$ to the same CP. The results are for a system size $N = 100$. In (a) the sequence of times is $t = 2, 10, 20, 26, 30, 40$ and in (b) $t = 2, 10, 20, 25, 30, 40$. Reproduced from Ref. [11].

like behavior while in the second case there is a constructive interference when the peaks of the evolved state meet at the center of the wire. Consistently with the results for the overlaps, in this regime the difference in energy between states with high weight halves, and the period doubles.

Both the revival time and the period of the oscillations are associated with the propagation of the state along the system, with a velocity that, in the case of a free system, travels at a velocity given by the quasiparticle energy slope [12]. In the case of interacting systems, it generalizes to a limiting velocity value, similar to a light-cone propagation [13–16].

A similar conclusion is obtained performing a Fourier analysis of the time evolution of the survival probability. This is shown in Fig. 8. While for small initial values of Δ the distribution is quite narrow around low frequencies, it changes significanly as Δ grows, becoming quite extended. In the Fourier decomposition the amplitudes, u_n, are for the frequencies with values $\omega_n = \pi(n-1)/N_t$, where N_t is the number of time points considered.

It is also interesting to study the survival probability of excited states, that in this problem are extended states throughout the chain. Close to the critical point the survival probability of most states is close to 1 except near the low energy modes. Further away from the critical point the deviation of the survival probability from unity extends to higher energy states due to the orthogonality between the eigenstates of the original and final

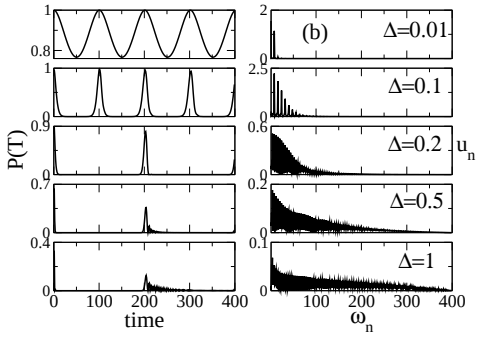

Fig. 8. Survival probability and its Fourier analysis for the $1D$ Kitaev model. Reproduced from Ref. [11].

Hamiltonians[11].

3.2. *Generation of Majorana states*

While quenches in general destabilize the edge states, due to the finiteness of a system, we may generate Majorana states through a sudden quench starting from a trivial phase. Even though in the thermodynamic limit the topological properties can not be changed by a unitary transformation[10,17], the probability that a given initial state in a trivial phase III may collapse to a Majorana of the final state Hamiltonian in phase I is finite and independent of time. Quenching to a state close to the transition line, the overlaps of several (extended) states are considerable due to the spatial extent of the Majorana states. If the quench is deeper into the topological phase these become more localized and the overlap decreases. Interestingly the larger overlap is found for some higher energy, extended states.

A sequence of quenches allows for the manipulation of the states[11]. A possibility to turn off and on Majoranas can be trivialy seen in the following way. Consider starting from a state inside region I of the phase diagram Fig. 1. Perform a critical quench to the line $\Delta = 0$ and then a quench back to the original state. Choosing appropriately t_1 we may get a state with no overlap with the initial Majoranas, as illustrated in Fig. 5. So we are back to a topological phase but with no edge states. But Majoranas may be switched back on if at a time $t_2 > t_1$ we perform another quench to a state in region I. Due to the quench to ξ_3 a finite probability to find the

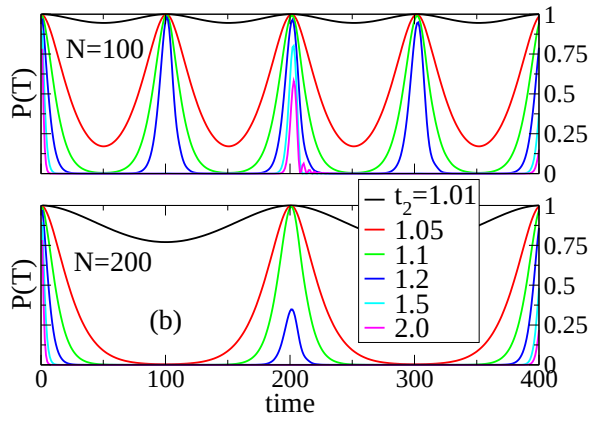

Fig. 9. (Color online) Survival probability of edge modes of the $1D$ Schockley model. Critical quenches are considered from the topological region to the transition point ($t_1 = t_2$). Reproduced from Ref. [11].

Majorana state is found [11] even though if no quench from $\xi_2 = \xi_0 \to \xi_3$ was performed, and having chosen appropriately t_1, the survival probability of the Majorana states was tuned to vanish. Note that the overlap of Majorana state of $H(\xi_3)$ with a Majorana state of $H(\xi_0)$ is finite, since the states are chosen to be close by.

4. Dynamics of $1D$ multiband systems

While in the previous section Majorana edge states of Kitaev's model were considered, edge states in other systems, including topological insulators, have also been considered and show similar properties. In this section we consider two topological systems, the Shockley model [3] which has fermionic edge states and no Majoranas, and the SSH-Kitaev model [5] which displays both types of edge states in different parts of the phase diagram, allowing a comparison of different edge state dynamics.

4.1. $1D$ *Shockley model*

In Fig. 9 we show critical quenches to a final state with $t_2 = t_1 = 1$ starting from different initial points in the topological region ($t_2 > t_1$). The cases

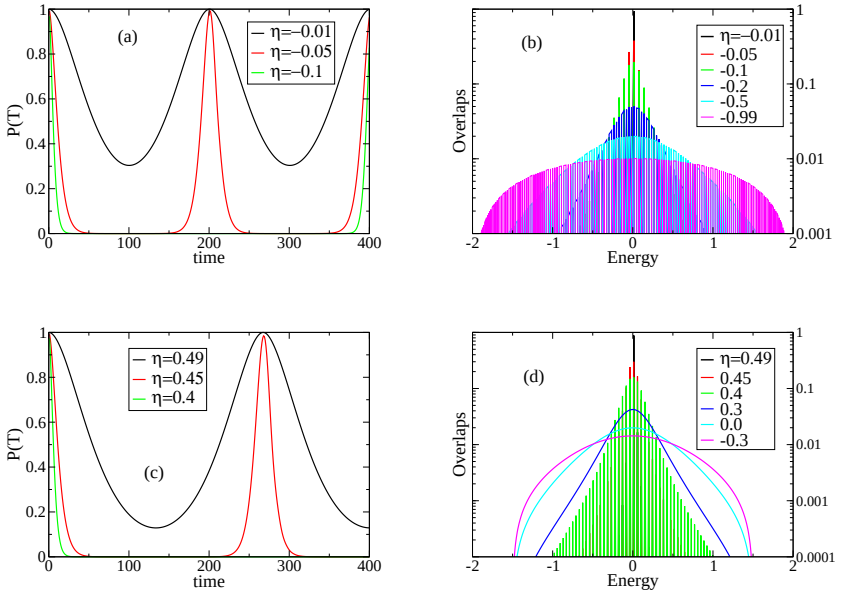

Fig. 10. (Color online) Critical quenches in the $1D$ SSH-Kitaev model: survival probability and overlaps. The CP on the first two panels is $\eta = 0, \Delta = 0$ (SSH2) and on the last two panels the CP is $\eta = 0.5, \Delta = 0.5$ (K1). Reproduced from Ref. [11].

of $N = 100$ and $N = 200$ are shown. As in the Kitaev model the period scales with the system size. The behavior is very similar to the Kitaev model. We see the period doubling for both cases for $t_2 = 1.5$. For $t_2 = 2.0$ the smoothness of the oscillations is replaced by a superposition of many frequencies. From the point of view of edge state dynamics the behavior of Majoranas and fermionic edge states are similar.

Also, moving further away from the critical point a behavior similar to Fig. 4b is seen with a rapid decrease of $P(t)$ and the appearance of revival times.

4.2. *1D SSH-Kitaev model*

The similarities between Majorana and fermionic edge states are further shown considering the SSH-Kitaev model. In Fig. 2 we showed the phase diagram of the SSH-Kitaev model[5] in the case of $\mu = 0$. In phase K1 we are in the Kitaev regime with one zero energy edge mode at each edge

(Majoranas). In the SSH regimes we are closer to the behavior of the SSH model with fermionic modes. In SSH 0 there are no edge modes. In SSH 2 there are two zero energy fermionic modes.

In Fig. 10 we consider critical quenches to points in the transition between different topological regions. In the top panels we consider $P(t)$ and the overlaps, respectively, of a transition at $\mu = 0$ from the SSH 2 regime to the critical point $\eta = 0, \Delta = 0$ by considering different initial values of $\eta = -0.01, -0.05, -0.1, -0.2, -0.5, -0.99$. In the lower panels we consider critical quenches to the critical point $\eta = 0.5, \Delta = 0.5$ changing the initial value of η. In both cases note that there is again a change of the distribution of the overlaps from sharp peaks, at small deviations from the critical point, to a broad distribution of the overlaps as one moves sufficiently away from the critical point; again there is a crossover between the two regimes (not shown), as for the Kitaev model. However, the overlaps are not smooth as a function of energy. Note that in the first case $\Delta = 0$, which means that this occurs in the context of the SSH model with no superconductivity. In the second case we have a mixture of SSH and Kitaev model, but the behavior is qualitatively similar in the crossover region. Beyond it we find again the very smooth distributions of the overlaps as in the Kitaev model.

5. Dynamics of edge states of 2D triplet superconductor

5.1. *Wave-function propagation*

The edge states appear if we consider a strip geometry of finite transversal width, N_y, with open boundary conditions (OBC) along y and periodic boundary conditions (PBC) along the longitudinal direction, x, of size N_x. The diagonalization of this Hamiltonian expressed in real space involves the solution of a $(4N_xN_y) \times (4N_xN_y)$ eigenvalue problem. The energy states include states in the bulk and states along the edges and are written in the form of a 4-component spinor as

$$\begin{pmatrix} u_n \\ v_n \end{pmatrix} = \begin{pmatrix} u_n(j_x, j_y, \uparrow) \\ u_n(j_x, j_y, \downarrow) \\ v_n(j_x, j_y, \uparrow) \\ v_n(j_x, j_y, \downarrow) \end{pmatrix}. \tag{30}$$

Here j_x, j_y are the spatial lattice coordinates along x and y, respectively. Focusing our attention on a Majorana mode, we present in Fig. 11 the time evolution of the absolute value of the spinor component $u_n(j_x, j_y, \uparrow)$, as an example, for a time evolution for $(M_z = 2, \mu = -5) \rightarrow (M_z = 0, \mu =$

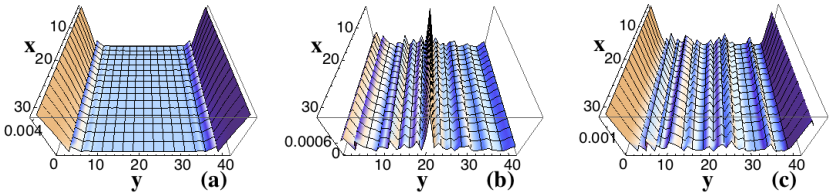

Fig. 11. (Color online) Time evolution of real space $|u_\uparrow|^2$ for $(M_z = 2, \mu = -5) \rightarrow (M_z = 0, \mu = -5)$ $C = 1 \rightarrow C = 0$ (trivial) for $t = 0, t = 50, t = 62$, shown in (a), (b), (c), respectively. Note that in these transitions there are no edge states in the final states. In the various panels the horizontal axis is the y direction and the vertical direction is the x direction. The system size is 31×41. Reproduced from Ref. [10].

$-5)$ $C = 1 \rightarrow C = 0$ (trivial) for $t = 0, t = 50, t = 62$, shown in (a), (b), (c), respectively. The other spinor components have a qualitatively similar behavior. A set of characteristic time values are selected (time is expressed in units of $1/\tilde{t}$). The initial state shows a mode that is very much peaked at the borders of the system and that decays fast inside the supercondutor along the transverse direction. As time evolves the peaks move towards the center until they merge at some later time, dependent of the system transverse size (as for the Kitaev model). After this time the peaks move back from the center, the wave functions become more extended as a mixture to all the eigenstates becomes more noticeable. Eventually at later times the wave function recovers a shape that is close to the initial state and there is a partial revival of the original state. The process then repeats itself but the same degree of coherence is somewhat lost. In Fig. 11 the quenches are carried out between a topological phase and a trivial phase $(C = 1 \rightarrow C = 0)$ and $(C = -2 \rightarrow C = 0)$. The behavior is therefore qualitatively the same as for the $1D$ case.

5.2. *Evolution of Chern numbers*

The topology of each phase may be characterized by the Chern number, defined over the Brillouin zone of the system [7]. As the system evolves in time, the wave functions change. Solving for the evolution of the wave functions we may calculate the Chern number as a function of time and determine how the topology changes as well. Due to the fluctuating evolution of the overlaps between a given state and all the others in the appropriate subspace, we may expect that wave functions over the Brillouin zone will fluctuate considerably as time goes by.

In Fig. 12 it is shown that the Chern number remains locked to the

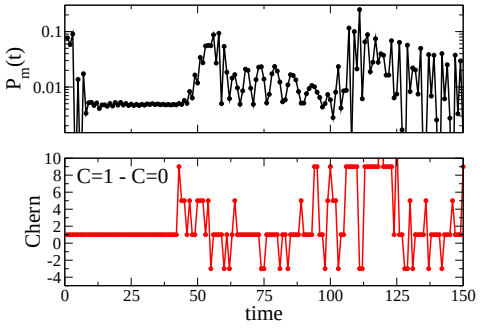

Fig. 12. (Color online) Comparison of time evolution of (a) survival probability and (b) Chern number for the case of strong spin orbit coupling for $(M_z = 2, \mu = -5) \rightarrow (M_z = 0, \mu = -5)$ corresponding to $C = 1 \rightarrow C = 0$. The Chern number remains stable at the initial state value until the Majorana mode reaches the middle point of the system. Beyond this instant the Chern number fluctuates. Reproduced from Ref. [10].

initial state value until the Majorana mode reaches the center point of the system and, therefore, the topology is maintained. Beyond that instant the Chern number starts to fluctuate which indicates that gaps are closing and opening due to the time evolution. In the thermodynamic limit the revival times extend to infinity and the Chern number does not change [10,17], even though the edge states do decay. However, the Chern number may change due to the finiteness of the system. The values taken by the Chern number at a given time can be quite large. Since the Chern numbers fluctuate considerably it may make sense to look at the time averaged Chern numbers. These average values have a very slow convergence to the value corresponding to the Chern value of the final state and is not conclusive if it fully occurs.

6. Periodic driving

A different type of time perturbation that has attracted considerable interest are periodic perturbations. While quenches, either abrupt or slow, in general destabilize the edge states, topological phases can be induced by periodically driving the Hamiltonian of a non-topological system, such as shown before in topological insulators [18–20] and in topological superconductors, with the appearance of Majorana fermions [21–24]. Their appearance in a one-dimensional p-wave superconductor was studied in Ref. [25] and in

Ref.[26] introducing external periodic perturbations; the case of intrinsic periodic modulation was also considered[27]. The periodic driving leads to new topological states[19], and to a generalization of the bulk-edge correspondence, that reveals a richer structure[28,29] as compared with the equilibrium situation[8,30]. Similarly, in topological superconductors new phases may be induced and manipulated due to the presence of the periodic driving[25,31,32], such as shining a laser on a topologically trivial system.

6.1. *Floquet formalism*

The time evolution of a state under the influence of a time dependent Hamiltonian is given by

$$i\frac{\partial}{\partial t}\psi(k,t) = H(k,t)\psi(k,t) \tag{31}$$

where k is the momentum, t the time and we take $\hbar = 1$. We can decompose the Hamiltonian in two terms: a time independent one, $H(k)$, and an extra term due to the external time-dependent perturbation, that we want to take as periodic with a given frequency, ω,

$$H(k,t) = H(k) + f(\omega t)H_d(k) \tag{32}$$

where $f(\omega t + 2\pi) = f(\omega t)$. Here $H_d(k)$ is of the form of the unperturbed Hamiltonian but with only one non-vanishing term. Looking for a solution of the type

$$\psi(k,t) = e^{-i\epsilon(k)t}\Phi(k,t) \tag{33}$$

and using that $\Phi(k,t) = \Phi(k,t+T)$, where T is the period ($\omega = 2\pi/T$), one gets that

$$\left(H(k,t) - i\frac{\partial}{\partial t}\right)\Phi(k,t) = \epsilon(k)\Phi(k,t) \tag{34}$$

The time-independent quasi-energies $\epsilon(k)$ are the eigenvalues of the operator $H(k,t) - i\frac{\partial}{\partial t}$ and the function $\Phi(k,t)$ the eigenfunction. Note that due to the external time dependent perturbation, energy is not conserved and therefore the original energy bands loose their meaning. Since this function is periodic, we can expand it as

$$\Phi(k,t) = \sum_m \phi_m(k)e^{im\omega t} \tag{35}$$

Inserting this expansion in equation 34 we obtain the time-independent eigensystem

$$\sum_{m'} H_{mm'}(k)\phi_{m'}(k) = \epsilon(k)\phi_m(k) \tag{36}$$

with the quasi-energies the eigenvalues. The Hamiltonian matrix is given by

$$H_{mm'}(k) = \delta_{mm'} m\omega + \frac{1}{T}\int_0^T dt e^{-im\omega t} H(k,t) e^{im'\omega t} \tag{37}$$

Choosing a perturbation of the type $f(\omega t) = \cos(\omega t)$ the second term of the Hamiltonian matrix reduces to $1/2\,(\delta_{m'+1,m} + \delta_{m'-1,m})$.

The time evolution of the state is then obtained solving for the quasi-energies, $\epsilon(k)$, and the functions $\phi_m(k)$ diagonalizing the infinite matrix

$$\begin{pmatrix} \cdots & \cdots & \cdots & \cdots & \cdots \\ \cdots & (m-1)\omega + H(k) & \frac{1}{2}H_d(k) & 0 & \cdots \\ \cdots & \frac{1}{2}H_d(k) & m\omega + H(k) & \frac{1}{2}H_d(k) & \cdots \\ \cdots & 0 & \frac{1}{2}H_d(k) & (m+1)\omega + H(k) & \cdots \\ \cdots & \cdots & \cdots & \cdots & \cdots \end{pmatrix} \tag{38}$$

The matrix can be reduced if the frequency is high enough and then only a few values of m are needed. In the case of a $2D$ triplet superconductor, hopping, chemical potential, spin-orbit coupling or magnetization, will be considered to vary with time. The first three parameters preserve time reversal symmetry while the magnetization naturally breaks time reversal symmetry if the unperturbed Hamiltonian is in a regime with vanishing magnetization. Emphasis will be placed on the effects of varying the chemical potential or the magnetization which are easilly tuned externally. In this last case it has been determined before[26] that even though the low energy states have a very low energy, they may not be strictly Majorana fermions since the eigenvalues of the Floquet operator (time evolution operator over one time period) are not strictly ± 1.

Due to the periodicity of the eigenfunctions, $\Phi(k, t+T) = \Phi(k,t)$, the action of the evolution operator, $\mathcal{U}(t)$, on a state over a period, T, leads to the same state minus a phase

$$|\psi(T)\rangle = \mathcal{U}(T)|\psi(0)\rangle = e^{-i\epsilon T}|\psi(0)\rangle \tag{39}$$

Therefore, the quasi-energies are defined minus a shift of a multiple of $w = 2\pi/T$, and we can restrict the quasi-energies to the first Floquet zone, defined by the interval $-w/2 \leq \epsilon \leq w/2$. States with quasi-energies $\epsilon =$

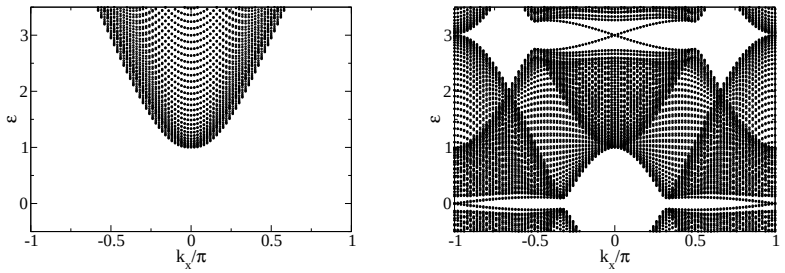

Fig. 13. Energy spectrum of (a) the unperturbed Hamiltonian (or Floquet spectrum for $l = 0$) and (b) Floquet spectrum for $l = 3$ for a d_x, d_y triplet superconductor in a topologically trivial phase $\alpha = 0.1, M_z = 0, \mu = -5, \Delta_s = 0.1, d_z = 0, d = 0.6$ where the magnetization is changed with time with frequency $w = 6$. The periodic driving is $M_{zd} \cos wt$ with $M_{zd} = 4$. Reproduced from Ref. [33].

$w/2$ and $\epsilon = -w/2$ are therefore equivalent and there is a reflection of any bands as one exits the Floquet zone from above (or below) and as one enters from below (or above). Considering the particle-hole symmetry of a superconductor, $\gamma_{-\epsilon} = \gamma_{\epsilon}^{\dagger}$ and the equivalence between the energies $\epsilon = -w/2, w/2$ one expects a new type of finite quasi-energy Majorana mode in addition to any zero energy states, the usual Majorana modes.

6.2. *Quasi-energy bands of 2D triplet superconductor*

The solutions for the quasi-energies of the perturbed Hamiltonians lead to bands that have a similar structure to the energy bands of the unperturbed Hamiltonian obtained taking a real space description with OBC along y and a momentum description along x.

At large frequencies, $w > 4\tilde{t}$, the size of the truncated matrix is relatively small and the quasi-energies and physical properties (calculated over the first Floquet zone) converge fast for small values of m. Considering $m = 0$ one reproduces the Hamiltonian of the unperturbed superconductor. The first approximation for the driven system is obtained considering $m = 1, 0, -1$, then $m = 2, 1, 0, -1, -2$ and so on. One may therefore use a short notation for the number of terms considered in the diagonalization of the Hamiltonian matrix by using $l = 0, 1, 2, 3, \cdots$. The unperturbed case is denoted by $l = 0$ and the perturbed cases by $l = 1, 2, \cdots$ (considering that we are using $2l + 1$ states). If the frequency w is small, one needs to consider large values of l and the problem of finding the edge states in a

ribbon geometry quickly becomes heavy computationally. Increasing the value of the frequency it is easy to find that it is enough to consider $l = 2$, since taking $l = 3$ leads to very similar results, with a good accuracy.

In Fig. 13 we consider periodic drivings in the magnetization for moderate couplings of $M_{zd} = 4$ and compare to the unperturbed case. We consider frequency $w = 6$. In this case the unperturbed system is in a trivial phase evidenced by the absence of gapless edge states inside the bulk gap. Adding the perturbation edge states appear at low energies and also appear at the border of the Floquet zone around $w/2$ (and $-w/2$). These states are also localized at the edges of the system. In general, edge states appear at the border of the Floquet zone, but as we can see from the figure there is no clearly defined gap throughout the Brillouin zone. Edge states at low energies do not always appear or are mixed with bulk edges. If the driving frequency is smaller or the perturbation has a small amplitude the convergence is slow and in general the quasi-energy spectrum is complex with a strong mixture of the edge and bulk states[33].

6.3. *Currents*

The edge states lead to the appearance of currents. The charge current operator along direction x at a given position $\hat{j}_y$ along y is given by[33]

$$\hat{j}_c(j_y) = \frac{2e}{\hbar} \sum_{k_x} \boldsymbol{\psi}^\dagger_{k_x,j_y} \begin{pmatrix} -\tilde{t}\sin(k_x) & -\frac{i}{2}\alpha\cos(k_x) \\ \frac{i}{2}\alpha\cos(k_x) & -\tilde{t}\sin(k_x) \end{pmatrix} \boldsymbol{\psi}_{k_x,j_y} \tag{40}$$

where $\boldsymbol{\psi}^\dagger_{k_x,j_y} = \left(\psi^\dagger_{k_x,j_y,\uparrow}, \psi^\dagger_{k_x,j_y,\downarrow}\right)$. The current has contributions from the hopping and the spin-orbit terms. The operators are written in real space along y and in momentum space along x. One may also define a longitudinal spin current, $\hat{j}_s(j_y)$, taking the difference between the two diagonal components of the charge current. The other terms correspond to spin-flip terms and do not contribute to the z component of the spin current.

The average value of the charge current in the groundstate is given by summing over the single particle occupied states (negative energies) in the

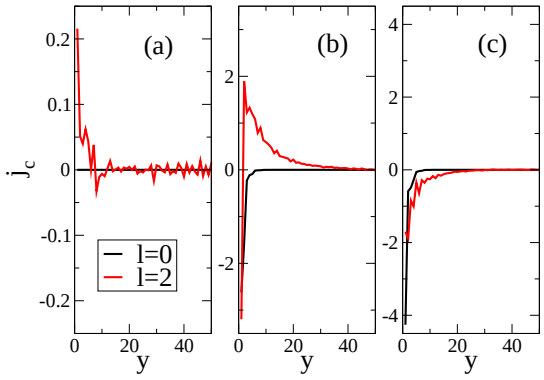

Fig. 14. (Color online) Charge current profiles for the unperturbed ($l = 0$) and perturbed ($l = 2$) d_x, d_y superconductor for (a) $\mu = -5, M_z = 0$ (with $C = 0$), (b) $\mu = -5, M_z = 2$ (with $C = 1$) and (c) $\mu = -1, M_z = 2$ (with $C = -2$) and for $\mu_d = 1$. Only one half of the system is shown since the current profile is anti-symmetric around the middle point. The system size is $N_y = 100$.

usual way

$$\begin{aligned} j_c(j_y) = \langle \hat{j}_c(j_y) \rangle = \sum_{k_x,n} \{ & \tilde{t} \sin k_x \, [\tilde{v}_n(-k_x, j_y, \uparrow)\tilde{v}_n^*(-k_x.j_y, \uparrow) \\ & + \tilde{v}_n(-k_x, j_y, \downarrow)\tilde{v}_n^*(-k_x.j_y, \downarrow)] \\ & - \frac{i\alpha}{2} \cos k_x \, [\tilde{v}_n(-k_x, j_y, \uparrow)\tilde{v}_n^*(-k_x.j_y, \downarrow) \\ & - \tilde{v}_n(-k_x, j_y, \downarrow)\tilde{v}_n^*(-k_x.j_y, \uparrow)] \} \end{aligned} \tag{41}$$

Here the functions are of the type

$$\tilde{u}_n(k_x, j_y, \sigma) = \sum_m e^{imwt} u_{n,m}(k_x, j_y, \sigma) \tag{42}$$

where as usual $\sigma = \uparrow, \downarrow$.

The charge currents at the edges of the unperturbed Hamiltonian are well understood. If there is TRS the currents vanish and if TRS is broken the edge charge currents are finite (finite Chern number). We consider as example a d_x, d_y triplet superconductor. If the magnetization vanishes, the system has TRS and vanishing charge edge currents in the topologically trivial phases. The charge current also vanishes in the Z_2 topological phase but the spin edge currents are non-vanishing.

We consider a set of parameters $d = 0.6, \Delta_s = 0.1, d_z = 0, \alpha = 0.6$ and different values for the chemical potential and the magnetization. In Fig. 14 we show results for the profile of the charge current as a function of y for various cases. We compare the unperturbed case with the perturbed one by considering that at $w = 6$ it is enough to truncate the Hamiltonian matrix at $l = 2$. To calculate the currents we sum over the states in the first Floquet zone. Also the results are for time $t = 0$ or any multiple of the time period T. As seen in Fig. 14a the periodic driving gives rise to a finite charge current that is absent in the unperturbed trivial phase. In the other two panels the edge states of the unperturbed system carry a finite current which is altered by the periodic driving due to the appearance of extra edge states and also a reshaping of the continuum states; notably there is a change of sign in Fig. 14b.

As shown in Ref.[33] the edge states also generate spin currents. Associated with the spin currents in the topological phases, it has been shown that the eigenstates have non trivial spin polarizations that depend strongly on the momentum[34]. In Ref.[33] the spin polarization of the induced edge states is also considered.

7. Conclusions

In this work the robustness of edge modes of topological systems to time-dependent perturbations was considered. The fermionic and Majorana edge mode dynamics of various topological systems were compared, after a global quench of the Hamiltonian parameters takes place. Also, the effect of a periodic perturbation was considered. In general the edge modes are not stable, however in finite systems there is the possibility of revival after a finite time. It was shown that the distinction due to the Majorana nature of the excitations plays a small role in comparison to the details of the energy spectrum and overlaps between states.

Slow transformations were not considered here but allow the occurence of the Kibble-Zurek mechanism of defect production as one crosses a quantum critical point. In the context of the Creutz ladder, it was shown before that the presence of edge states modifies the process of defect production expected from the Kibble-Zurek mechanism, leading in this problem to a scaling with the change rate with a non-universal critical exponent[35]. A similar result was obtained for the one-dimensional superconducting Kitaev model, where it was shown that, although bulk states follow the Kibble-Zurek scaling, the produced defects for an edge state quench are quite anomalous and

independent of the quench rate[36]. Similar results have been found for a $2D$ triplet superconductor[10]. As in the case of sudden quenches, there seems to be no particular signature of the Majorana fermions in comparison to other edge modes. Note that Majoranas are absent in the Creutz ladder.

Fermionic edge states in a topological insulator are now established[37]. Even though Majorana edge states have been extensively studied in the literature their experimental detection has proved challenging. While there is promising evidence of Majorana edge states[38,39] in magnetic chains superimposed on a conventional superconductor, there may be other sources of the edge states observed in the system considered (see for instance ref.[40] for a discussion and references therein).

One of the methods proposed to detect the presence of Majorana edge states is the measurement of the differential conductance at the interface between a lead and a topological superconductor. If the lead is metallic one expects a zero-bias peak in the differential conductance, if zero-energy modes are present in the superconducting side. In the presence of Majorana modes one expects a vanishing conductance if the number of Majorana modes is even and a quantized value of $2e^2/h$, if the number of modes is odd[41,42]. In the case of the dimerized SSH model here considered, it has been shown[5] that the fermionic edge modes do not contribute to the conductance and, therefore, provides a method to distinguish the various phases and the type of edge modes.

Acknowledgements

The author acknowledges discussions with Pedro Ribeiro, Antonio Garcia-Garcia, Xiaosen Yang, Maxim Dzero and Henrik Johannesson. Partial support in the form of a BEV by the CNPq at CBPF (Rio de Janeiro) and partial support and hospitality by the Department of Physics of Gothenburg University are acknowledged. Partial support from the Portuguese FCT under Grants No. PEST- OE/FIS/UI0091/2011, No. PTDC/FIS/111348/2009 and UID/CTM/04540/2013 is also acknowledged.

References

1. M. Z. Hasan and C. L. Kane, Rev. Mod. Phys. **82**, 3045 (2010)
2. J. Alicea, Rep. Prog. Phys. **75**, 076501 (2012).
3. S.S. Pershoguba and V.M. Yakovenko, Phys. Rev. B **86**, 075304 (2012).
4. A.Y. Kitaev, Phys.-Usp. **44**, 131 (2001).

5. R. Wakatsuki, M. Ezawa, Y. Tanaka and N. Nagaosa, Phys. Rev. B **90**, 014505 (2014).
6. T.O. Puel, P.D. Sacramento and M.A. Continentino, J. Phys. Cond. Matt. **27**, 422002 (2015).
7. M. Sato and S. Fujimoto, Phys. Rev. B **79**, 094504 (2009).
8. A.P. Schnyder, S. Ryu, A. Furusaki and A.W.W. Ludwig, Phys. Rev. B **78**, 195125 (2008; A.P. Schnyder, S. Ryu, A. Furusaki and A.W.W. Ludwig, in *Advances in Theoretical Physics*, edited by Vladimir Lebedev and Mikhail Feigel'man, AIP Conf. Proc. No. 1134 (AIP, Melville, NY, 2009), p. 10; S. Ryu, A.P. Schnyder, A. Furusaki and A.W.W. Ludwig, New J. Phys. **12**, 065010 (2010).
9. A. Rajak and A. Dutta, Phys. Rev. E **89**, 042125 (2014).
10. P. D. Sacramento, Phys. Rev. E **90**, 032138 (2014).
11. P. D. Sacramento, Phys. Rev. E **93**, 062117 (2016).
12. J. Happola, G. B. Halasz and A. Hamma, Phys. Rev. B **85**, 032114 (2012).
13. E. H. Lieb and D. W. Robinson, Comm. Math. Phys. **28**, 251 (1972).
14. S. Bravyi, M. B. Hastings, and F. Verstraete, Phys. Rev. Lett. **97**, 050401 (2006).
15. M. Cheneau, P. Barmettler, D. Poletti, M. Endres, P. Schau, T. Fukuhara, C. Gross, I. Bloch, C. Kollath, and S. Kuhr, Nature **481**, 484 (2012).
16. L. Bonnes, F. H. L. Essler, and A. M. Laüchli, Phys. Rev. Lett. **113**, 187203 (2014).
17. L. D'Alessio and M. Rigol, Nat. Comm. **6**, 8336 (2015).
18. Takashi Oka and Hideo Aoki, Phys. Rev. B **79**, 081406(R) (2009).
19. N.H. Lindner, G. Refael and V. Galitski, Nat. Phys. **7**, 490 (2011).
20. J.I. Inoue and A. Tanaka, Phys. Rev. Lett. **105**, 017401 (2010); T. Kitagawa, E. Berg, M. Rudner and E. Demler, Phys. Rev. B **82**, 235114 (2010)
21. L. Jiang, T. Kitagawa, J. Alicea, A.R. Akhmerov, D. Pekker, G. Refael, J.I. Cirac, E. Demler, M.D. Lukin and P. Zoller, Phys. Rev. Lett. **106**, 220402 (2011).
22. Qing-Jun Tong, Jun-Hong An, Jiangbin Gong, Hong-Gang Luo, and C. H. Oh, Phys. Rev. B **87**, 201109(R) (2013).
23. Xiaosen Yang, arXiv:1410.5035.
24. A. Poudel, G. Ortiz, and L. Viola, Europhys. Lett. **110**, 17004 (2015).
25. D.E. Liu, A. Levchenko and H.U. Baranger, Phys. Rev. Lett. **111**, 047002 (2013).

26. M. Thakurathi, A.A. Patel, D. Sen and A. Dutta, Phys. Rev. B **88**, 155133 (2013).
27. M.S. Foster, V. Gurarie, M. Dzero and E.A. Yuzbashyan, Phys. Rev. Lett. **113**, 076403 (2014).
28. Mark S. Rudner, Netanel H. Lindner, Erez Berg, and Michael Levin, Phys. Rev. X **3**, 031005 (2013).
29. Gonzalo Usaj, P. M. Perez-Piskunow, L. E. F. Foa Torres, and C. A. Balseiro, Phys. Rev. B **90**, 115423 (2014).
30. J.K. Asbóth, B. Tarasinski and P. Delplace, Phys. Rev. B **90**, 125143 (2014).
31. M. Benito, A. Gmez-Len, V. M. Bastidas, T. Brandes, and G. Platero. Phys. Rev. B **90**, 205127 (2014).
32. Zi-Bo Wang, Hua Jiang, Haiwen Liu, and X. C. Xie, Sol. Stat. Commun. **215-216**, 18 (2015).
33. P. D. Sacramento, Phys. Rev. B **91**, 214518 (2015).
34. Andreas P. Schnyder, Carsten Timm, and P. M. R. Brydon, Phys. Rev. Lett. **111**, 077001 (2013).
35. A. Bermudez, D. Patanè, L. Amico and M.A. Martin-Delgado, Phys. Rev. Lett. **102**, 135702 (2009).
36. A. Bermudez, L. Amico and M.A. Martin-Delgado, New Journ. Phys. **12**, 055014 (2010).
37. B. Bernevig, T. Hughes and S. Zhang, Science **314**, 1757 (2006).
38. V. Mourik, K. Zuo, S. M. Frolov, S. R. Plissard, E. P. A. M. Bakkers, and L. P. Kouwenhoven, Science **336**, 1003 (2012).
39. Stevan Nadj-Perge, Ilya K. Drozdov, Jian Li, Hua Chen, Sangjun Jeon, Jungpil Seo, Allan H. MacDonald, B. Andrei Bernevig and Ali Yazdani, Science **346**, 602 (2014).
40. E. Dumitrescu, B. Roberts, S. Tewari, J. D. Sau, and S. Das Sarma, Phys. Rev. B **91**, 094505 (2015).
41. K.T. Law, P.A. Lee and T.K. Ng, Phys. Rev. Lett. **103**, 237001 (2009).
42. M. Wimmer, A.R. Akhmerov, J.P. Dahlhaus and C.W.J. Beenakker, New J. Phys. **13**, 053016 (2011).